


Solving conformal defects in 3D conformal field theory using fuzzy sphere regularization

Received: 23 November 2023

Liangdong Hu ^{1,2}, Yin-Chen He ³  & W. Zhu ¹ 

Accepted: 17 April 2024

Published online: 30 April 2024

 Check for updates

Defects in conformal field theory (CFT) are of significant theoretical and experimental importance. The presence of defects theoretically enriches the structure of the CFT, but at the same time, it makes it more challenging to study, especially in dimensions higher than two. Here, we demonstrate that the recently-developed theoretical scheme, *fuzzy (non-commutative) sphere regularization*, provides a powerful lens through which one can dissect the defect of 3D CFTs in a transparent way. As a notable example, we study the magnetic line defect of 3D Ising CFT and clearly demonstrate that it flows to a conformal defect fixed point. We have identified 6 low-lying defect primary operators, including the displacement operator, and accurately extract their scaling dimensions through the state-operator correspondence. Moreover, we also compute one-point bulk correlators and two-point bulk-defect correlators, which show great agreement with predictions of defect conformal symmetry, and from which we extract various bulk-defect operator product expansion coefficients. Our work demonstrates that the fuzzy sphere offers a powerful tool for exploring the rich physics in 3D defect CFTs.

Defects, as well as their special case—boundaries, are fundamental elements that inevitably exist in nearly all realistic physical systems. Historically, research on defects has played a pivotal role in shaping modern theoretical physics. This includes contributions to the theory of the renormalization group (RG)¹, studies of topological phases^{2–4}, investigations into the confinement of gauge theories^{5,6}, explorations of quantum gravity⁷, and advancements in the understanding of quantum entanglement^{8,9}. An important instance to study defects is in the context of conformal field theory (CFT)^{10,11}, where one considers the situation of deforming a CFT with interactions living on a sub-dimensional defect. The defect may trigger an RG flow towards a non-trivial infrared (IR) fixed point, which can still have an emergent conformal symmetry defined on the space-time dimensions of the defect^{12–17}. The theory describing such a conformal defect is called a defect CFT (dCFT) (see refs. 18,19 for recent discussions). Understanding dCFTs is an important step in comprehending CFTs in nature, as most experimental realizations of CFTs necessarily accompany defects (and boundaries). Moreover, dCFTs have a non-trivial interplay

with the bulk CFTs, and knowledge of the former will advance the understanding of the latter. For example, the two-point correlators of bulk operators in dCFT constrain and encode the conformal data of the bulk CFT²⁰, similar to the well-known story of four-point correlators of a bulk CFT.

dCFTs are typically richer and more intricate than their bulk CFT counterparts. On one hand, for a given bulk CFT, there exist multiple (even potentially infinite) distinct dCFTs, and their classification remains an open challenge. On the other hand, breaking of the full conformal symmetry group into a subgroup renders the study of dCFTs more challenging, as the space-time conformal symmetry becomes less restrictive, making modern approaches like the conformal bootstrap program²¹ less powerful^{20,22–25}. Notably, most of the well-established results concerning dCFTs are confined to 2D CFTs, including the seminal results on the boundary operator contents¹³ and RG flow²⁶, thanks to the special integrability property of 2D CFTs. In comparison, higher-dimensional CFTs pose greater difficulties, and the knowledge of dCFTs in dimensions beyond two is rather limited.

¹Department of Physics, School of Science, Westlake University, Hangzhou 310030, PR China. ²Institute of Natural Sciences, Westlake Institute for Advanced Study, 18 Shilongshan Road, Hangzhou 310024, PR China. ³Perimeter Institute for Theoretical Physics, Waterloo, ON N2L 2Y5, Canada.

 e-mail: yhe@perimeterinstitute.ca; zhuwei@westlake.edu.cn

Current studies of dCFTs mainly revolve around perturbative RG computations^{27–34} and Monte Carlo simulations of lattice models^{18,35–37}. An important progress made recently is the non-perturbative proof of RG monotonic g-theorem in 3D and higher dimensions^{38,39}, generalizing the original result in 2D^{26,40,41}.

In the context of dCFTs, many important questions remain to be answered, ranging from basic inquiries such as the existence of conformal defect fixed points to more advanced queries concerning the infrared properties of dCFTs, including their conformal data such as critical exponents. The central aim of this paper is to develop an efficient tool for the non-perturbative analysis of 3D dCFTs. Specifically, we extend the success of the recently proposed fuzzy sphere regularization⁴² from bulk CFTs^{42–45} to the realm of dCFTs. As a concrete example, we explore the properties of the 3D Ising CFT in the presence of a magnetic line defect^{32–36,46–49}. We directly demonstrate that this line defect indeed flows to an attractive conformal fixed point, and we identify 6 low-lying defect primary operators with their scaling dimensions extracted through the state-operator correspondence. Furthermore, we study the one-point bulk primary correlators and the two-point bulk-defect correlators, both of which are fixed by conformal invariance, up to a set of operator product expansion (OPE) coefficients. As far as we know, most of conformal data of dCFT reported here have never been studied before. In this context, our paper not only presents a comprehensive set of results concerning the magnetic line defect in the 3D Ising CFT, but also lays the foundation for further exploration of 3D dCFTs using the fuzzy sphere regularization technique.

Results

Conformal defect and radial quantization

We consider a 3D CFT deformed by a p -dimensional defect, described by the Hamiltonian

$$H_{CFT} + h \int d^p r \mathcal{O}(r). \tag{1}$$

Examples include the line defect ($p = 1$, see Fig. 1a) and the plane defect ($p = 2$). If the defect is not screened in the IR, the system will flow into a non-trivial fixed point that breaks the original conformal symmetry $SO(4,1)$ of H_{CFT} . Furthermore, if the non-trivial fixed point is still conformal, such a defect is called a conformal defect described by a dCFT. For such a dCFT, the original conformal group is broken down to a smaller subgroup $SO(p+1,1) \times SO(3-p)$ ^{17–19}, where $SO(p+1,1)$ is the conformal symmetry of the defect, and $SO(3-p)$ is the rotation symmetry around the defect that acts as a global symmetry on the defect.

A dCFT possesses a richer structure compared to its bulk counterpart. Firstly, there is a set of operators living on the defect, forming representations of the defect conformal group $SO(p+1,1)$. Furthermore, there are non-trivial correlators between bulk operators and defect operators. (Hereafter, we follow the usual convention and denote the defect operator with a hat \hat{O} , while the bulk operator is represented as O without a hat.) The simplest example is that the bulk primary operator gets a non-vanishing one-point correlator, which is in sharp contrast to the bulk CFT^{17–19}:

$$\langle O_1(x) \rangle = \frac{a_{O_1}}{|x_\perp|^{\Delta_1}}. \tag{2}$$

Here, $|x_\perp|$ is the perpendicular distance from the bulk operator to the defect, Δ_1 is the scaling dimension of O_1 , and a_{O_1} is an operator-dependent universal number (we consider the case of O_1 to be a Lorentz scalar). Moreover, we can consider a bulk-defect two-point (scalar-scalar) correlator defined as^{17–19}:

$$\langle O_1(x) \hat{O}_2(0) \rangle = \frac{b_{O_1 \hat{O}_2}}{|x_\perp|^{\Delta_1 - \Delta_2} |x|^{\Delta_2}}, \tag{3}$$

where $b_{O_1 \hat{O}_2}$ is the bulk-defect OPE coefficient. Interestingly, the bulk two-point correlator already becomes non-trivial, and its functional form cannot be completely fixed by the conformal symmetry.

Similar to the bulk CFT, we consider the radial quantization of a dCFT. Specifically, we first foliate the Euclidean space \mathbb{R}^3 using spheres S^2 with their origins situated on the defect, as illustrated in Fig. 1a. Next, we can perform a Weyl transformation to map \mathbb{R}^3 to a cylinder $S^2 \times \mathbb{R}$, and the p -dimensional defect transforms into a defect intersecting the cylinder. For instance, as shown in Fig. 1, the Weyl transformation maps a line defect ($p = 1$) in \mathbb{R}^3 to 0 + 1D point impurities located at the north and south poles of the sphere S^2 , forming two continuous line cuts along the time direction from $\tau = -\infty$ to $\tau = \infty$. Similarly, a plane defect ($p = 2$) in \mathbb{R}^3 will be mapped to a 1 + 1D defect with its spatial component located on the equator of the sphere S^2 .

Akin to the state-operator correspondence in bulk CFT^{50,51}, we have a one-to-one correspondence between the defect operators and the eigenstates of the dCFT quantum Hamiltonian on $S^2 \times \mathbb{R}$, where energy gaps of these states are proportional to the scaling dimensions $\hat{\Delta}_n$ of the defect operators:

$$E_n - E_0 = \frac{v}{R} \hat{\Delta}_n. \tag{4}$$

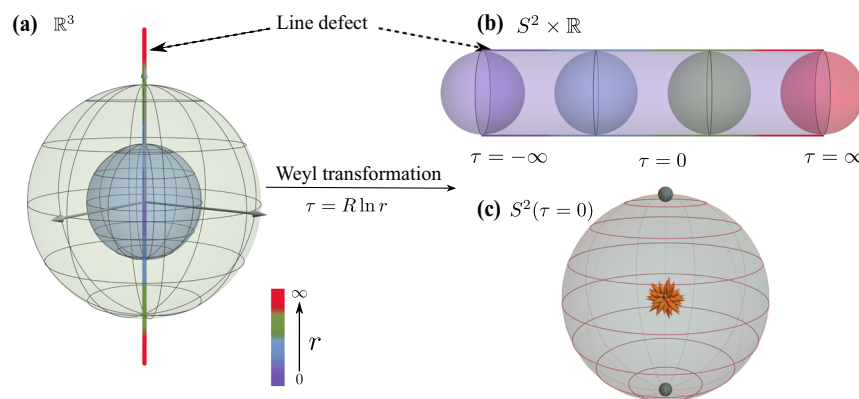


Fig. 1 | Schematic plot of the defect in 3D. Through a Weyl transformation, a Euclidean flat space-time \mathbb{R}^3 is mapped to (b) the cylinder manifold $S^2 \times \mathbb{R}$. The line defect before and after the Weyl transformation are shown by the colored line.

c The 0 + 1-D impurities (cyan point) located at the north and south pole on two-dimensional sphere S^2 in the radial quantization, where the flux at the center represents the magnetic monopole defined in the fuzzy sphere model.

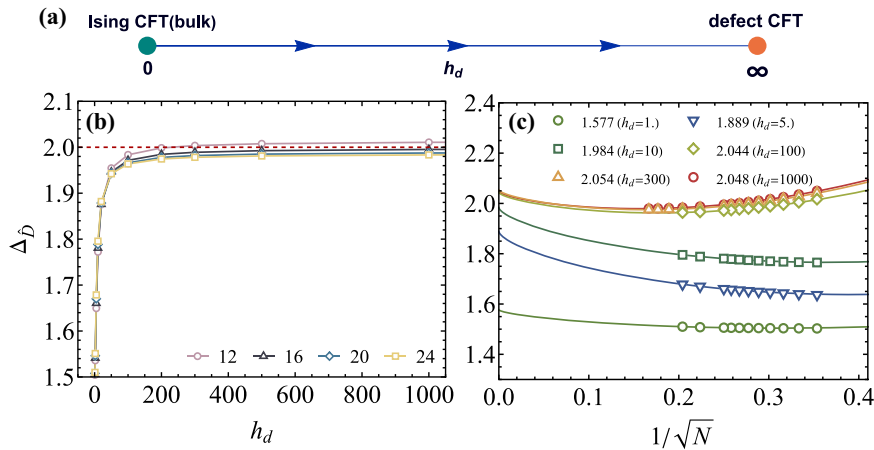


Fig. 2 | Defect induced attractive fixed point. **a** Schematic plot of the RG diagram. **b** The scaling dimension of displacement operator Δ_D as a function of defect strength h_d . Different colored symbols represent the results based on various system sizes. **c** Finite-size extrapolation of Δ_D for various h_d (see Supplementary

Note 2 and 3 in Supplementary Material). A sufficient large h_d gives almost identical $\Delta_D \approx 2$, supporting an attractive RG fixed point at $h_d = \infty$. Different colored symbols represent the results based on various defect strength h_d .

Here, E_0 denotes the ground state energy of the defect Hamiltonian, R represents the sphere radius, and v is a model-dependent non-universal velocity that corresponds to the arbitrary normalization of the Hamiltonian. Notably, this velocity v is identical to the velocity of the bulk CFT Hamiltonian (further discussions see Supplementary Note 2 in Supplementary Material).

The state-operator correspondence offers distinct advantages for studying CFTs. Firstly, it provides direct access to information regarding whether the conformal symmetry emerges in the IR. Secondly, it enables an efficient extraction of various conformal data, such as scaling dimensions and OPE coefficients of primaries. The key step involves studying a quantum Hamiltonian on the sphere geometry. However, for 3D CFTs, this was challenging as no regular lattice could fit S^2 . Recently, this fundamental obstacle was overcome through a scheme called “fuzzy sphere regularization”⁴², and its superior capabilities have been convincingly demonstrated^{42–45}. Below we discuss how to adapt the fuzzy sphere regularization scheme to solve dCFTs. We will focus on the case of magnetic line defect of the 3D Ising CFT, but the generalizations to other cases should be straightforward.

Magnetic line defect on the fuzzy sphere

The fuzzy sphere regularization⁴² considers a quantum mechanical model describing fermions moving on a sphere with a $4\pi s$ magnetic monopole at the center. The model is generically described by a Hamiltonian $H = H_{\text{kin}} + H_{\text{int}}$, where H_{kin} represents the kinetic energy of fermions, and its eigenstates form quantized Landau levels described by the monopole Harmonics $Y_{n+s,m}^{(s)}(\theta, \varphi)$ ⁵². Here, $n = 0, 1, \dots$ denotes the Landau level index, and (θ, φ) are the spherical coordinates. We consider the limit where H_{kin} is much larger than the interaction H_{int} , allowing us to project the system onto the lowest Landau level (i.e. $n = 0$), resulting in a fuzzy sphere⁵³.

The 3D Ising transition on the fuzzy sphere can be realized by two-flavor fermions $\psi^\dagger = (\psi_1^\dagger, \psi_2^\dagger)$ with interactions that mimic a 2+1D transverse Ising model on the sphere,

$$H_0 = \int R^4 d\Omega_a d\Omega_b U(\Omega_{ab})(n^0(\Omega_a)n^0(\Omega_b) - n^z(\Omega_a)n^z(\Omega_b)) - h \int R^2 d\Omega n^x(\Omega). \quad (5)$$

Here we are using the spherical coordinate $\Omega = (\theta, \varphi)$ and R is the sphere radius. The density operators are defined as $n^a(\Omega) = \psi^\dagger(\Omega) \sigma^a \psi(\Omega)$, where $\sigma^{x,y,z}$ are the Pauli matrices and σ^0 is the identity matrix. $U(\Omega_{ab})$ encodes the Ising density-density interaction as $U(\Omega_{ab}) = \frac{g_0}{R^2} \delta(\Omega_{ab}) + \frac{g_1}{R^4} \nabla^2 \delta(\Omega_{ab})$. One can tune the transverse field h

to realize a phase transition which falls into the 2+1D Ising universality class⁴². In the following, we set $U(\Omega_{ab})$ and h the same as the bulk Ising CFT that has been identified in⁴².

To study the magnetic line defect of 3D Ising CFT, we add 0 + 1D point-like magnetic impurities located at sphere’s north and south pole, modeled by a Hamiltonian term,

$$H_d = 2\pi h_d (n^z(\theta = 0, \varphi = 0) + n^z(\theta = \pi, \varphi = 0)), \quad (6)$$

where h_d controls the strength of the magnetic impurities. This type of defect can be artificially realized in experiments^{54,55}. Crucially, the defect term H_d breaks the Ising \mathbb{Z}_2 symmetry, causing the σ field (of the 3D Ising CFT) to be turned on at the defect. This σ deformation is relevant on the line defect ($\Delta_\sigma \approx 0.518 < 2$), driving the system to flow to a nontrivial fixed point, conjectured to be a conformal defect. This fixed point is expected to be an attractive fixed point^{32–34}, implying that regardless of the strength of h_d , the defect will flow to the same conformal defect fixed point (see Fig. 2a). Next we will provide compelling numerical evidence to support this conjecture.

Emergent conformal symmetry and operator spectrum

The energy spectrum of the defect Hamiltonian ($H_0 + H_d$) is expected to be proportional to the defect operators’ scaling dimensions, up to a non-universal velocity in Eq. (4). Here we determine the velocity using the bulk CFT Hamiltonian (H_0) by setting the σ state to have $\Delta_\sigma = 0.518149$ ²¹. The defect term H_d breaks the sphere rotation $SO(3)$ down to $SO(2)$, so each eigenstate has a well defined $SO(2)$ quantum number L_z . Akin to the stress tensor of the bulk CFT, there exists a special primary operator in dCFT due to the broken of translation symmetry, dubbed the displacement operator $\hat{D}^{17–19}$, which has $L_z = \pm 1$ and a protected scaling dimension $\Delta_D = 2$. Fig. 2b, c depicts Δ_D via the state-operator correspondence (Eq. (4)) for various defect strength h_d and system sizes. It clearly shows that the obtained Δ_D are very close to 2, for different defect strengths h_d , which indicates an attractive conformal fixed point at $h_d = \infty$ (see Supplementary Note 3 and 6 in Supplementary Material). In what follows, we present the representative results for $h_d = 300$ and we ensure the conclusions are insensitive to the choice of h_d .

We further establish the emergent conformal symmetry by confirming that the excitation spectra form representations of $SO(2, 1)$. The generators of $SO(2, 1)$ are the dilation D , translation P , and special conformal transformation K . It is important to note that P and K do not have any Lorentz index due to the triviality of the Lorentz symmetry,

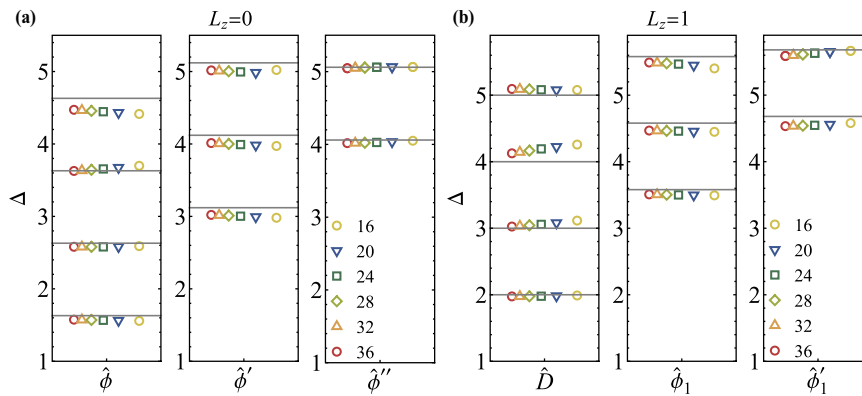


Fig. 3 | Conformal tower of defect primaries. Defect primary fields and their descendants with global symmetry (a) $L_z = 0$ and (b) $L_z = 1$. The gray horizon lines stand for extrapolated values for primaries and their integer-spaced descendants. Different colored symbols represent the results based on various system sizes. By

increasing system size N all of the scaling dimensions approach the theoretical values consistently, supporting an emergent conformal symmetry in the thermodynamic limit.

i.e., $SO(1)$. For each primary operator, we have descendants generated by the translation, $P^n \hat{O}$, whose scaling dimension is $\Delta_{P^n \hat{O}} = \Delta_{\hat{O}} + n$, and its $SO(2)$ quantum number L_z remains unchanged. Figure 3 displays our numerical data of the low-lying energy spectrum, clearly exhibiting the emergent conformal symmetry, i.e., approximate integer spacing between each primary and its descendants. These observations firmly establish that the magnetic line defect of the 3D Ising CFT flows to a conformal defect with a conformal symmetry of $SO(2, 1)$.

From our numerical data, we can identify five low-lying defect primary operators in addition to \hat{D} , as listed in Table 1. Notably, all these operators are found to be irrelevant (i.e., $\Delta > 1$), which is consistent with the observation of an attractive defect fixed point. Our lowest-lying operator $\hat{\phi}$ has $L_z = 0$ and $\Delta_{\hat{\phi}} \approx 1.63(6)$. This value is in good agreement with Monte Carlo simulations, e.g. $1.60(5)^{36}$, $1.52(6)^{36}$, and $1.40(3)^{35}$, as well as with the perturbative ϵ -expansion computation of $\sim 1.55(14)$ ref. 34. The second low-lying operator in the $L_z = 0$ sector has $\Delta_{\hat{\phi}'} = 3.12(10)$, which significantly deviates from the ϵ -expansion value of $\Delta \approx 4.33 + O(\epsilon^2)$ (it was called \hat{s}_+ in³⁴). This suggests a large sub-leading correction in the ϵ -expansion. All other primary operators identified in our study have not been computed by any other methods. It is essential to mention that the scaling dimensions in Table 1 are obtained by the finite-size extrapolating (see details in Supplementary Note 2 in Supplementary Material), and the data at finite N is already very close to the extrapolated value (The finite-size extrapolation improve the results by around 2%). One can also improve the accuracy by making use of conformal perturbation⁵⁶.

Additionally, to verify the physics of dCFT presented here is independent of the specific value h_d , we directly study the spectrum at $h_d = \infty$ (see Supplementary Note 6 in Supplementary Material). Comparing it with the results at $h_d = 300$, we found them to be consistent with each other. This result indicates that the large h_d regime shares the same dCFT and also supports that the fixed point of dCFT indeed resides at $h_d = \infty$.

Table 1 | Scaling dimensions of primary operators in the magnetic line defect of 3D Ising CFT, determined through the state-operator correspondence on the fuzzy sphere

$L_z = 0$			$L_z = 1$		
$\hat{\phi}$	$\hat{\phi}'$	$\hat{\phi}''$	\hat{D}	$\hat{\phi}_1$	$\hat{\phi}'_1$
1.63(6)	3.12(10)	4.06(18)	2.05(7)	3.58(7)	4.64(14)

Please see a detailed analysis of errors and finite-size extrapolation in Supplementary Note 2 and 3 in Supplementary Material.

Correlators and OPE coefficients

Using Weyl transformation, we can map the bulk-defect correlators in Eq. (2), Eq. (3) in \mathbb{R}^3 to the correlators on cylinder $S^2 \times \mathbb{R}$ (see Supplementary Note 1 in Supplementary Material),

$$G_{O_1, \hat{O}_2} \equiv \frac{\langle \hat{1} | O_1(\tau=0, \theta) | \hat{O}_2 \rangle}{\langle \hat{1} | O_1(\tau=0, \theta) | O_1 \rangle} = \frac{b_{O_1, \hat{O}_2}}{(\sin \theta)^{\Delta_1 - \Delta_2}}. \quad (7)$$

The bulk operator O_1 is positioned at a point that has an angle θ with respect to the north pole. In the denominator, we use the states of the bulk CFT, while in the numerator, we use the states of the dCFT. The one-point bulk correlator corresponds to taking $|\hat{O}_2\rangle$ to be the ground state of the defect, i.e., $|\hat{1}\rangle$.

In the fuzzy sphere model, we can use the spin operators n^z and n^x to approximate the bulk CFT primary operators σ and ϵ ^{43,44}. For example, the correlator between the bulk primary σ and a defect primary operator \hat{O}_2 is computed by,

$$G_{\sigma, \hat{O}_2} \equiv \frac{\langle \hat{1} | n^z(\tau=0, \theta) | \hat{O}_2 \rangle}{\langle \hat{1} | n^z(\tau=0, \theta) | \sigma \rangle} = \frac{b_{\sigma, \hat{O}_2}}{(\sin \theta)^{\Delta_\sigma - \Delta_2}} + O(N^{-1/2}). \quad (8)$$

Here, $\Delta_\sigma \approx 0.518149$, and the first-order correction $O(N^{-1/2})$ comes from the descendant operator $\partial_\mu \sigma$ contained in n^z . Figure 4 illustrates the one-point bulk correlator $G_\sigma(\theta)$ and bulk-defect correlator $G_{\sigma, \hat{\phi}}(\theta)$ for different system sizes $N = 12-36$. Both correlators agree perfectly with the CFT prediction Eq.(7), except for the small θ regime. It is worth noting that the one-point correlator $G_\sigma(\theta)$ is divergent at $\theta = 0, \pi$ and reaches a minimum at $\theta = \pi/2$. In contrast, the bulk-defect correlator $G_{\sigma, \hat{\phi}}(\theta)$ has an opposite behavior (because $\Delta_\sigma - \Delta_{\hat{\phi}} < 0$); it vanishes at $\theta = 0, \pi$ and reaches a maximum at $\theta = \pi/2$. These behaviors are nicely reproduced in our data, which is highly nontrivial because computationally the only difference for the two correlators is the choice of $|\hat{O}_2\rangle$ in Eq. (8).

We can further extract the bulk-defect OPE coefficients from $G_{O_1, \hat{O}_2}(\theta = \pi/2) = b_{O_1, \hat{O}_2}$, and the results are summarized in Table 2. None of these OPE coefficients was computed non-perturbatively before. There are perturbative computations for a_σ and a_ϵ ³⁴ from ϵ expansion, giving $a_\sigma^2 \approx 3.476 + O(\epsilon^2)$ (i.e. $a_\sigma \approx 1.86$) and $a_\epsilon \approx 1.83 + O(\epsilon^2)$. Our estimates are $a_\sigma = 1.37(1)$ and $a_\epsilon = 1.31(19)$, it will be interesting to compute higher order corrections in the ϵ -expansion. Moreover, using the Ward identity of any bulk operator (O)¹⁹,

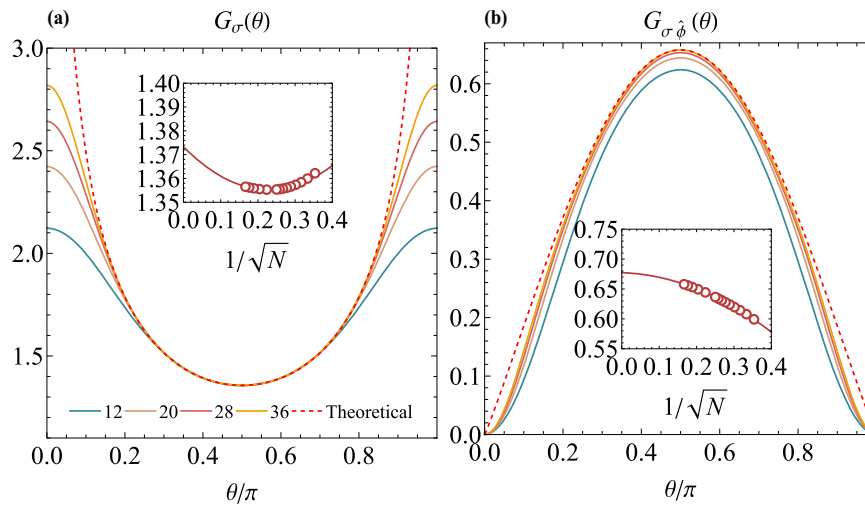


Fig. 4 | Correlators involving defect. The angle dependence of (a) correlator $G_\sigma(\theta)$ and (b) $G_{\sigma\hat{\phi}}(\theta)$, for system sizes ranging from $N=12$ – 36 . The dashed lines correspond to theoretical correlator in Eq. (7) with $b_{\sigma\hat{o}_2}$ and $\Delta_{\hat{o}_2}$ from the $N=36$ curves.

The insets are finite-size scaling analysis by setting $\theta = \pi/2$, respectively giving one-point OPE coefficient $a_\sigma \approx 1.37(1)$ and bulk-defect OPE coefficient $b_{\sigma\hat{\phi}} \approx 0.68(1)$.

we can extract Zamolodchikov norm

$$\sqrt{C_D} = \frac{2}{\pi} \frac{\Delta_O G_O(\theta = \pi/2)}{G_{OD}(\theta = \pi/2)}. \quad (9)$$

The estimates using σ and ϵ gives $C_D = 0.53(3)$ and $C_D = 0.59(18)$, respectively.

Discussion

We have outlined a systematic procedure to study defect conformal field theory (dCFT) using the recently proposed fuzzy sphere regularization scheme. As a concrete application, we investigated the magnetic line defect of 3D Ising CFT and provided clear evidence that it flows to a conformal defect. Crucially, we accurately computed a number of conformal data of this dCFT, including defect primaries' scaling dimensions and bulk-defect OPE coefficients. As far as we know, most of the conformal data of dCFT reported here have never been studied in a microscopic model before, thus this conformal information paves the way for exploring the rich physics in 3D Ising CFTs.

Looking forward, the current setup can be readily applied to the study of various types of defects in distinct 3D CFTs, potentially resolving numerous open questions and offering insights into defects in CFTs. For example, the plane defect ($p=2$ in Eq. (1)), which may resemble surface critical phenomena, is interesting to investigate. It is also highly desired to study 3D dCFTs in a broad universality class (e.g. Wilson–Fisher $O(N)$ critical point). Moreover, the results of current work provide a necessary input in the study of infrared data for the dCFT within the numerical conformal bootstrap^{20–22}. Taking it further would potentially be very interesting to study the dCFT in holography and string theory.

Table 2 | Bulk-to-defect OPE coefficients magnetic line defect of 3D Ising CFT

a_σ	$b_{\sigma\hat{\phi}}$	a_ϵ	$b_{\epsilon\hat{\phi}}$	C_D by σ	C_D by ϵ
1.37(1)	0.68(1)	1.31(19)	1.63(4)	0.53(3)	0.59(18)

C_D is computed by Eq. (9) using σ and ϵ .

Methods

The model $H_0 + H_d$ for the magnetic line defect of 3D Ising CFT is a continuous model with fully local interaction in the spatial space. In practice, we consider the second quantization form of this model by the projecting $H_0 + H_d$ to the lowest Landau level (fuzzy sphere), using $\psi_a(\Omega) = \frac{1}{\sqrt{N}} \sum_{m=-s}^s c_{m,a} Y_{s,m}^{(s)}(\Omega)$ (we are using a slightly different convention compared to ref. 42). Here $N=2s+1$ playing the role of system size $N \sim R^2$, and we simply replace R^2 with N during the projection. This lowest Landau level projection leads to a second quantized Hamiltonian defined by fermionic operators $c_{m,a}$ and similar models have been extensively studied in the context of the quantum Hall effect⁵⁷. Numerically, this model can be simulated using various techniques such as exact diagonalization and density matrix renormalization group (DMRG)^{58,59}. We perform DMRG calculations with bond dimensions up to $D=5000$, and for the largest system size $N=36$, the maximum truncation errors for the ground state and the tenth excited state are 1.37×10^{-9} and 1.96×10^{-8} , respectively. We explicitly impose two $U(1)$ symmetries, i.e., fermion number and $SO(2)$ angular momentum.

Data availability

All data are included in this published article and Supplementary Information files.

Code availability

The codes used to generate data and plots are available from the corresponding author upon request. The DMRG data are generated using the software “ITensor 3(C++ Version)”⁶⁰.

References

- Wilson, K. G. The renormalization group: Critical phenomena and the kondo problem. *Rev. Mod. Phys.* **47**, 773–840 (1975).
- Nayak, C., Simon, S. H., Stern, A., Freedman, M. & Das Sarma, S. Non-abelian anyons and topological quantum computation. *Rev. Mod. Phys.* **80**, 1083–1159 (2008).
- Hasan, M. Z. & Kane, C. L. Colloquium: Topological insulators. *Rev. Mod. Phys.* **82**, 3045–3067 (2010).
- Qi, X.-L. & Zhang, S.-C. Topological insulators and superconductors. *Rev. Mod. Phys.* **83**, 1057–1110 (2011).
- Wilson, K. G. Confinement of quarks. *Phys. Rev. D* **10**, 2445–2459 (1974).

6. Hooft, Gerard't On the phase transition towards permanent quark confinement. *Nucl. Phys. B* **138**, 1–25 (1978).
7. Maldacena, J. The large- n limit of superconformal field theories and supergravity. *Int. J. Theor. Phys.* **38**, 1113–1133 (1999).
8. Holzhey, C., Larsen, F. & Wilczek, F. Geometric and renormalized entropy in conformal field theory. *Nucl. Phys. B* **424**, 443–467 (1994).
9. Calabrese, P. & Cardy, J. Entanglement entropy and quantum field theory. *J. Stat. Mech.* **2004**, P06002 (2004).
10. Philippe Francesco, David Sénéchal, Mathieu, P. *Conformal Field Theory, Graduate Texts in Contemporary Physics* (Springer, 1997).
11. Cardy, J., *Scaling and Renormalization in Statistical Physics* (Cambridge University Press, 1996).
12. Cardy, J. L. Conformal invariance and surface critical behavior. *Nucl. Phys. B* **240**, 514–532 (1984).
13. Cardy, J. L. Boundary conditions, fusion rules and the verlinde formula. *Nucl. Phys. B* **324**, 581–596 (1989).
14. Cardy, J. L. & Lewellen, D. C. Bulk and boundary operators in conformal field theory. *Phys. Lett. B* **259**, 274–278 (1991).
15. Diehl, H. W. & Dietrich, S. Field-theoretical approach to multicritical behavior near free surfaces. *Phys. Rev. B* **24**, 2878–2880 (1981).
16. McAvity, D. M. & Osborn, H. Energy-momentum tensor in conformal field theories near a boundary. *Nucl. Phys. B* **406**, 655–680 (1993).
17. McAvity, D. M. & Osborn, H. Conformal field theories near a boundary in general dimensions. *Nucl. Phys. B* **455**, 522–576 (1995).
18. Billó, M. et al. Line defects in the 3d Ising model. *J. High Energy Phys.* **2013**, 55 (2013).
19. Billó, M., Gonçalves, V., Lauria, E. & Meineri, M. Defects in conformal field theory. *J. High Energy Phys.* **2016**, 91 (2016).
20. Liendo, P., Rastelli, L. & van Rees, B. C. The bootstrap program for boundary CFT_d. *J. High Energy Phys.* **2013**, 113 (2013).
21. Poland, D., Rychkov, S. & Vichi, A. The conformal bootstrap: Theory, numerical techniques, and applications. *Rev. Mod. Phys.* **91**, 015002 (2019).
22. Gaiotto, D., Mazac, D. & Paulos, M. F. Bootstrapping the 3d Ising twist defect. *J. High Energy Phys.* **2014**, 100 (2014).
23. Gliozzi, F., Liendo, P., Meineri, M. & Rago, A. Boundary and Interface CFTs from the Conformal Bootstrap. *J. High Energy Phys.* **2015**, 36 (2015).
24. Padayasi, J., Krishnan, A., Metlitski, M., Gruzberg, I. & Meineri, M. The extraordinary boundary transition in the 3d O(N) model via conformal bootstrap. *SciPost Phys.* **12**, 190 (2022).
25. Gimenez-Grau, A., Lauria, E., Liendo, P. & van Vliet, P. Bootstrapping line defects with O(2) global symmetry. *J. High Energy Phys.* **2022**, 18 (2022).
26. Affleck, I. & Ludwig, Andreas W. W. Universal noninteger “ground-state degeneracy” in critical quantum systems. *Phys. Rev. Lett.* **67**, 161–164 (1991).
27. Vojta, M., Buragohain, C. & Sachdev, S. Quantum impurity dynamics in two-dimensional antiferromagnets and superconductors. *Phys. Rev. B* **61**, 15152–15184 (2000).
28. Metlitski, M. A., Boundary criticality of the O(N) model in $d = 3$ critically revisited. *arXiv* <https://doi.org/10.48550/arXiv.2009.05119> (2020).
29. Liu, S., Shapourian, H., Vishwanath, A. & Metlitski, M. A. Magnetic impurities at quantum critical points: Large- N expansion and connections to symmetry-protected topological states. *Phys. Rev.* **104**, 104201 (2021).
30. Krishnan, A. and Metlitski, M. A., A plane defect in the 3d O(N) model. *arXiv* <https://doi.org/10.48550/arXiv.2301.05728> (2023).
31. Aharony, O., Cuomo, G., Komargodski, Z., Mezei, M. ár & Raviv-Moshe, A. Phases of Wilson Lines in Conformal Field Theories. *Phys. Rev. Lett.* **130**, 151601 (2023).
32. Hanke, A. Critical adsorption on defects in ising magnets and binary alloys. *Phys. Rev. Lett.* **84**, 2180–2183 (2000).
33. Allais, A. & Sachdev, S. Spectral function of a localized fermion coupled to the wilson-fisher conformal field theory. *Phys. Rev. B* **90**, 035131 (2014).
34. Cuomo, G., Komargodski, Z. & Mezei, M. ár Localized magnetic field in the O(N) model. *J. High Energy Phys.* **2022**, 134 (2022).
35. Allais, A., Magnetic defect line in a critical Ising bath. *arXiv* <https://doi.org/10.48550/arXiv.1412.3449> (2014).
36. Parisen Toldin, F., Assaad, F. F. & Wessel, S. Critical behavior in the presence of an order-parameter pinning field. *Phys. Rev. B* **95**, 014401 (2017).
37. Parisen Toldin, F. & Metlitski, M. A. Boundary Criticality of the 3D O(N) Model: From Normal to Extraordinary. *arXiv* **128**, 215701 (2022).
38. Cuomo, G., Komargodski, Z. & Raviv-Moshe, A. Renormalization Group Flows on Line Defects. *Phys. Rev. Lett.* **128**, 021603 (2022).
39. Casini, H., Landea, I. S. & Torroba, G. Entropic g Theorem in General Spacetime Dimensions. *Phys. Rev. Lett.* **130**, 111603 (2023).
40. Friedan, D. & Konechny, A. Boundary Entropy of One-Dimensional Quantum Systems at Low Temperature. *Phys. Rev. Lett.* **93**, 030402 (2004).
41. Casini, H., Landea, I. S. & Torroba, G. The g-theorem and quantum information theory. *J. High Energy Phys.* **2016**, 140 (2016).
42. Zhu, W., Han, C., Huffman, E., Hofmann, J. S. & He, Yin-Chen Uncovering conformal symmetry in the 3d ising transition: State-operator correspondence from a quantum fuzzy sphere regularization. *Phys. Rev. X* **13**, 021009 (2023).
43. Hu, L., He, Y.-C. & Zhu, W. Operator product expansion coefficients of the 3d ising criticality via quantum fuzzy spheres. *Phys. Rev. Lett.* **131**, 031601 (2023).
44. Han, C., Hu, L., Zhu, W., and He, Yin-Chen, Conformal four-point correlators of the 3D Ising transition via the quantum fuzzy sphere. *arXiv* <http://arxiv.org/abs/2306.04681> (2023).
45. Zhou, Z., Hu, L., Zhu, W., and He, Yin-Chen, The SO(5) Deconfined Phase Transition under the Fuzzy Sphere Microscope: Approximate Conformal Symmetry, Pseudo-Criticality, and Operator Spectrum. *arXiv*, <https://doi.org/10.48550/arXiv.2306.16435> (2023).
46. Nishioka, T., Okuyama, Y. & Shimamori, S. The epsilon expansion of the O(N) model with line defect from conformal field theory. *J. High Energy Phys.* **2023**, 203 (2023).
47. Bianchi, L., Bonomi, D. & de Sabbata, E. Analytic bootstrap for the localized magnetic field. *J. High Energy Phys.* **2023**, 69 (2023).
48. Gimenez-Grau, A., Probing magnetic line defects with two-point functions. *arXiv*, <https://doi.org/10.48550/arXiv.2212.02520> (2022).
49. Pannell, W. H. & Stergiou, A. Line defect RG flows in the ϵ expansion. *J. High Energy Phys.* **2023**, 186 (2023).
50. Cardy, J. L. Conformal invariance and universality in finite-size scaling. *J. Phys. A* **17**, L385–L387 (1984).
51. Cardy, J. L. Universal amplitudes in finite-size scaling: generalisation to arbitrary dimensionality. *J. Phys. A* **18**, L757–L760 (1985).
52. Wu, T. T. & Yang, C. N. Dirac monopole without strings: monopole harmonics. *Nucl. Phys. B* **107**, 365–380 (1976).
53. Madore, J. The fuzzy sphere. *Classical Quantum Gravity* **9**, 69 (1992).
54. Law, B. M. Wetting, adsorption and surface critical phenomena. *Progr. Surface Sci.* **66**, 159–216 (2001).
55. Fisher, M. E. & de Gennes, P.-G. Phénomènes aux parois dans un mélange binaire critique. *Simple Views on Condensed Matter*, 237–241, https://doi.org/10.1142/9789812564849_0025 (2003).
56. Lao, B. -X. & Rychkov, S. 3D Ising CFT and Exact Diagonalization on Icosahedron. *arXiv*, <https://doi.org/10.48550/arXiv.2307.02540> (2023).
57. Haldane, F. D. M. Fractional quantization of the hall effect: A hierarchy of incompressible quantum fluid states. *Phys. Rev. Lett.* **51**, 605–608 (1983).
58. White, S. R. Density matrix formulation for quantum renormalization groups. *Phys. Rev. Lett.* **69**, 2863–2866 (1992).

59. Feiguin, A. E., Rezayi, E., Nayak, C. & Das Sarma, S. Density matrix renormalization group study of incompressible fractional quantum hall states. *Phys. Rev. Lett.* **100**, 166803 (2008).
60. Fishman, M., White, S. R., and Stoudenmire, E. M., *The ITensor Software Library for Tensor Network Calculations* (SciPost Phys. Codebases 4, 2022).

Acknowledgements

We thank Davide Gaiotto for stimulating discussions that initiated this project. L.D.H. and W.Z. were supported by National Natural Science Foundation of China (No. 92165102, 11974288) and National key R&D program (No. 2022YFA1402204). Research at Perimeter Institute is supported in part by the Government of Canada through the Department of Innovation, Science and Industry Canada and by the Province of Ontario through the Ministry of Colleges and Universities. YCH thanks the hospitality of Bootstrap 2023 at ICTP South American Institute for Fundamental Research, where part of this project was done.

Author contributions

W.Z. and Y.-C.H. initiated the project, L.D.H. performed the simulations. All authors contributed equally to the analysis of the data and writing of the manuscript.

Competing interests

The authors declare no competing interests.

Additional information

Supplementary information The online version contains supplementary material available at <https://doi.org/10.1038/s41467-024-47978-y>.

Correspondence and requests for materials should be addressed to Yin-Chen He or W. Zhu.

Peer review information *Nature Communications* thanks Gabriel Francisco Cuomo, and the other, anonymous, reviewer for their contribution to the peer review of this work. A peer review file is available

Reprints and permissions information is available at <http://www.nature.com/reprints>

Publisher's note Springer Nature remains neutral with regard to jurisdictional claims in published maps and institutional affiliations.

Open Access This article is licensed under a Creative Commons Attribution 4.0 International License, which permits use, sharing, adaptation, distribution and reproduction in any medium or format, as long as you give appropriate credit to the original author(s) and the source, provide a link to the Creative Commons licence, and indicate if changes were made. The images or other third party material in this article are included in the article's Creative Commons licence, unless indicated otherwise in a credit line to the material. If material is not included in the article's Creative Commons licence and your intended use is not permitted by statutory regulation or exceeds the permitted use, you will need to obtain permission directly from the copyright holder. To view a copy of this licence, visit <http://creativecommons.org/licenses/by/4.0/>.

© The Author(s) 2024